EurJIC
European Journal of Inorganic Chemistry

Full Papers
doi.org/10.1002/ejic.202100178

Chemistry Europe
European Chemical Societies Publishing

VIP *Very Important Paper*

Theoretical Investigation of Hydrogen-Bond-Assisted Tetradentate N4 Copper(I) Chloride and *trans*-1,2-Peroxodicopper Complexes

Min Zhang,[a] Guangchao Liang,*[b] and Mengjiang Xing[c, d]

Biological oxygenation catalyzed by copper-containing enzymes involves a dicopper O_2 adduct as the key intermediate. Significant insights were offered by the *trans*-1,2-peroxodicopper intermediates. To understand the activity of the *trans*-1,2-peroxodicopper intermediate in the oxygenation, a series of hydrogen-bond-assisted $Cu^{I}(L)$–Cl and *trans*-1,2-peroxodicopper complexes $[Cu_2–O_2]^{2+}$ were investigated by DFT computations. A reasonable two-parameter structure-activity model (R^2 = 0.8611) and a three-parameter structure-activity model (R^2 = 0.8773) for chloride dissociation (ΔG^1_{RXN}) were established. The critical intramolecular out-sphere hydrogen bonds assist the formation of stable *trans*-1,2-peroxodicopper complexes, which overcome the steric hindrances and electrostatic repulsion. An acceptable two-parameter structure-activity model (R^2 = 0.7051) for O_2 binding (ΔG^2_{RXN}) was obtained. The fundamental structure-activity interpretation of the hydrogen bonding interactions provides an insight into the modelling of *trans*-1,2-peroxodicopper mimics.

Introduction

The oxygenation via the O_2 activation by copper-containing enzymes is a critical process in the biological system.[1] The copper O_2 adduct is demonstrated as the key component in several copper-dependent enzymes, such as the hemocyanin, tyrosinase, and catechol oxidase.[2] The copper-oxygen moieties presented in the enzymes were mimicked by a variety of molecular copper complexes to understand their activities, mechanisms, and the structure-function relationships.[3] Formation of a stable dicopper O_2 adduct intermediate is one of the most essential challenges, which was addressed by the functional outer-sphere coordination. The involvement of such outer-sphere hydrogen bonding lights a bright way to the formation of dicopper O_2 adducts, especially the formation of *trans*-1,2-peroxodicopper complex.[4] The recent studies from Szymczak and co-workers showed that modification of the parent TPA [tris(2-pyridylmethyl)amine] ligand to TPA^{NHPh} [tris(6-phenylamino-2-pyridylmethyl)amine] (Scheme 1) with outer-sphere hydrogen bonds successfully led to the formation of related *trans*-1,2-peroxodicopper complex, $[\{Cu(TPA^{NHPh})\}_2(\mu\text{-}1,2\text{-}O_2)]^{2+}[BAr^-]_2$ [BAr=$B(C_6F_5)_4^-$] (Scheme 1).[5]

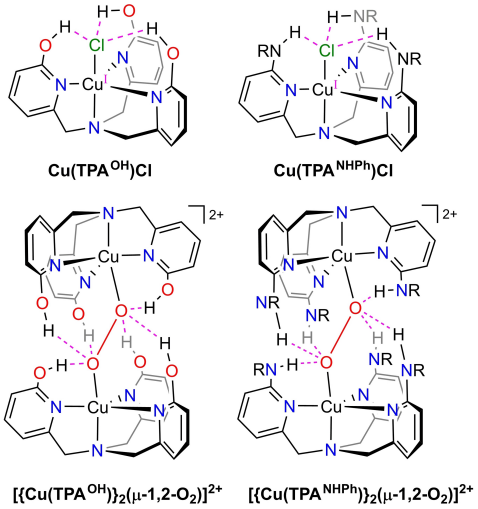

Scheme 1. Hydrogen-bond stabilized Cu–Cl and *trans*-1,2-peroxodicopper complexes. R=Ph.

The favorable hydrogen bonding interactions are considered as the dominant factor in the formation of the bulky *trans*-1,2-peroxodicopper $[\{Cu(TPA^{NHPh})\}_2(\mu\text{-}1,2\text{-}O_2)]^{2+}[BAr^-]_2$ complex via the reaction of $[Cu(TPA^{NHPh})]^+[BAr]$ with dry O_2 in CH_2Cl_2 solution at −70 °C, and the proximal and distal hydrogen bonds were confirmed by its solid-state X-ray structure.[5] The critical outer-sphere hydrogen bonds were also demonstrated in the $Cu^{I}(TPA^{OH})Cl$ complex [TPA^{OH} = tris(6-hydroxyl-2-pyridylmethyl)-amine].[6] The O–H···Cl hydrogen bonds stabilized Cu^{I}–Cl bond in $Cu^{I}(TPA^{OH})Cl$ was confirmed by its solid-state X-ray structure. The Cu–$N_{(axial)}$ and Cu–Cl bond distances in the $Cu^{I}(TPA^{OH})Cl$ are 2.238 and 2.566 Å, respectively, and the Cu–$N_{(axial)}$ and Cu–Cl

[a] *Dr. M. Zhang*
Department of Chemistry
Mississippi State University
Mississippi State, Mississippi 39762, United States
[b] *Dr. G. Liang*
Department of Chemistry
University of Michigan
Ann Arbor, Michigan 48109, United States
E-mail: gcliang@umich.edu
https://lsa.umich.edu/chem
[c] *Prof. M. Xing*
State Key Laboratory of Electronic Thin Films and Integrated Devices
University of Electronic Science and Technology of China
Chengdu, 610054, P. R. China
[d] *Prof. M. Xing*
Yangtze Delta Region Institute (Huzhou)
University of Electronic Science and Technology of China
Huzhou, 313001, P. R. China

Supporting information for this article is available on the WWW under https://doi.org/10.1002/ejic.202100178

bond distances in $[Cu^{II}(TPA^{OH})Cl]^+[PF_6]$ are 1.990 and 2.263 Å, respectively. B3LYP/Def-TZVP computations showed that the chloride dissociation in $Cu^{I}(TPA^{OH})Cl$ generating the axially vacant $[Cu(TPA^{OH})]^+$ (24.3 kcal mol^{-1}) was 18 kcal mol^{-1} higher than that in the parent $Cu^{I}(TPA)Cl$ (6.3 kcal mol^{-1}), which was due to the more stable Cu–Cl bond in $Cu^{I}(TPA^{OH})Cl$ induced by the hydrogen bonding interactions.[6]

These promising results from the outer-sphere hydrogen-bond assisted *trans*-1,2-peroxodicopper complexes provide a feasible and reliable strategy to explore the dicopper O_2 adduct intermediate in the oxygenation. It is noted that a structure-activity model is needed to promote the design of more stable *trans*-1,2-peroxodicopper analogues. To fully understand the effects of the introduced outer-sphere hydrogen bonds and to obtain the structure-activity model, a series of hydrogen bond assisted Cu^{I}–Cl and *trans*-1,2-peroxodicopper complexes (Scheme 2) were mimicked via DFT (density functional theory) computations. The parent $Cu^{I}(TPA)Cl$ complex[7] (complex **1**) and eight hydrogen bond assisted Cu^{I}–Cl complexes are included in Scheme 2. Complex **2** is the reported $Cu^{I}(TPA^{OH})Cl$,[6] and complex **9** is the reported $Cu^{I}(TPA^{NHPh})Cl$.[5] Complexes **3**–**8** [**3**, $Cu^{I}(TPA^{NH2})Cl$;[8] **4**, $Cu^{I}(TPA^{NHMe})Cl$; **5**, $Cu^{I}(TPA^{NHCF3})Cl$; **6**, $Cu^{I}(TPA^{NH2Me})Cl$; **7**, $Cu^{I}(TPA^{NH2CF3})Cl$; **8**, $Cu^{I}(TPA^{NHPhCF3})Cl$)] contain the N–H···Cl hydrogen bonds, and the N–H···Cl hydrogen bonds were formed by the pendent amine/substituted amines and Cl atom. The chloride dissociation in the $Cu^{I}(L)$–Cl complexes (ΔG^1_{RXN}, Scheme 2) and the formation of *trans*-1,2-peroxodicopper complexes $[Cu_2–O_2]^{2+}$ via O_2 binding to the $[Cu(L)]^+[BAr^-]$ (ΔG^2_{RXN}, Scheme 2) are discussed.

Theoretical Methods

Gas-phase geometry optimizations were carried out via Gaussian 16 package (Revision C 01)[9] with PBEPBE[10] functional and the Ahlrichs Def-TZVP[11] basis sets. Grimme's D3[12] dispersion with Becke-Johnson damping (D3BJ)[13] and density fitting approximation[14] (via the keyword AUTO) with pure spherical harmonic 5*d* and 7*f* functions were utilized. All located minima except the Cl^- anion via single-point computation were verified by vibrational frequency computations and no imaginary frequency was presented. The Gaussian 16 default ultrafine integration grid, 2-electron integral accuracy of 10^{-12}, and SCF convergence criterion of 10^{-8} were used for all computations. Szymczak and co-workers reported that the EPR (X-band) spectrum of *trans*-1,2-peroxodicopper complex $[\{Cu(TPA^{NHPh})\}_2(\mu\text{-}1,2\text{-}O_2)]^{2+}[BAr^-]_2$ [BAr=$B(C_6F_5)_4^-$] (Scheme 1) is silent,[5] which suggests the observed *trans*-1,2-peroxodicopper complex is a singlet complex. It is consistent with other *trans*-1,2-peroxodicopper complexes,[3b] and also supported by the reported theoretical studies.[3f,15] In order to approximately model the solvation effect in dichloromethane, the self-consistent reaction field (SCRF) single-point computations with Ahlrichs redefined Def2-TZVP[16] basis sets using the solvation model based on density (SMD)[17] based on the gas-phase optimized geometries were performed (SMD-PBEPBE-D3BJ/Def2-TZVP//PBEPBE-D3BJ/Def-TZVP). The Gibbs reaction energies for the Cl^- anion dissociation from $Cu^{I}(L)$–Cl species were calculated at 1 atm and 298.15 K, and the Gibbs reaction energies for formation of peroxodicopper complexes from the O_2 binding to the Cu^{I} species were calculated at 1 atm and 203.15 K. The electron density of bond critical point [$\rho_{(BCP)}$] based on Bader's theory of atoms-in-molecules (AIM)[18] and the core-valence bifurcation (CVB) index[19] were calculated by Multiwfn package (version 3.7)[20] and were visualized by VMD package (version 1.9.3).[21] The 3D molecular structures were created via Cambridge Structural Database (CSD) Mercury package (version 4.0.0).[22] The SambVca (version 2.1)[23] web application was used to illuminate the steric hindrance of ligand with parameters of percentages of buried volume (%V_{Bur})[24] and the steric map (see details in SI).[25]

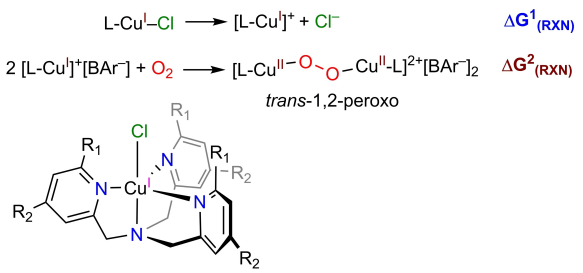

1: R_1 = H, R_2 = H — $\Delta G^1_{(RXN)}$ = 12.2, $\Delta G^2_{(RXN)}$ = –7.1
2: R_1 = OH, R_2 = H — $\Delta G^1_{(RXN)}$ = 26.4, $\Delta G^2_{(RXN)}$ = –16.0
3: R_1 = NH_2, R_2 = H — $\Delta G^1_{(RXN)}$ = 13.8, $\Delta G^2_{(RXN)}$ = –5.7
4: R_1 = $NHCH_3$, R_2 = H — $\Delta G^1_{(RXN)}$ = 15.6, $\Delta G^2_{(RXN)}$ = –11.1
5: R_1 = $NHCF_3$, R_2 = H — $\Delta G^1_{(RXN)}$ = 22.7, $\Delta G^2_{(RXN)}$ = –5.0
6: R_1 = NH_2, R_2 = CH_3 — $\Delta G^1_{(RXN)}$ = 13.9, $\Delta G^2_{(RXN)}$ = –9.2
7: R_1 = NH_2, R_2 = CF_3 — $\Delta G^1_{(RXN)}$ = 18.1, $\Delta G^2_{(RXN)}$ = –1.9
8: R_1 = NH(*p*-$PhCF_3$), R_2 = H — $\Delta G^1_{(RXN)}$ = 18.8, $\Delta G^2_{(RXN)}$ = –15.1
9: R_1 = NHPh, R_2 = H — $\Delta G^1_{(RXN)}$ = 13.6, $\Delta G^2_{(RXN)}$ = –11.6

Scheme 2. The Gibbs reaction energies for the model complexes. Gibbs energies from (SMD)-PBEPBE-D3BJ/Def2-TZVP//PBEPBE-D3BJ/Def-TZVP computations are given in kcal mol^{-1}.

Results and Discussion

The reliability of computational methodology (PBEPBE-D3BJ/Def-TZVP) in the ground state geometry optimization was verified firstly. DFT optimized gas-phase geometries of complexes $[\{Cu(TPA^{NHPh})\}_2(\mu\text{-}1,2\text{-}O_2)]^{2+}$, $[\{Cu(TPA)\}_2(\mu\text{-}1,2\text{-}O_2)]^{2+}$, $Cu^{I}(TPA^{NHPh})Cl$ and $Cu^{I}(TPA)Cl$ were compared with reported X-ray crystal structures (CSD entries: LELNUO, GECRAH, LELNOI, GIHWIE). The RMSD (root-mean-square deviation of atomic positions in Å) of the superposed structures for all non-hydrogen atoms were 0.0937, 0.1360, 0.2581, and 0.2232, respectively (Table S1). These observed reasonable RMSD values demonstrated the reliability of PBEPBE-D3BJ/Def-TZVP computations in the geometry optimization.

Chloride dissociation (ΔG^1_{RXN})

Copper(I) complexes with tetradentate N-donor ligands usually have trigonal pyramidal copper centers, forming the axially

Table 1. The calculated $\rho_{(BCP)}$ (a.u.) of N–H···Cl hydrogen bond and $\rho_{(BCP)}$ (a.u.) of Cu–Cl bond in Cu^{I}(L)–Cl.

Bond	1	2	3	4	5	6	7	8	9
N–H···Cl	0.0108	0.0397	0.0313	0.0320	0.0354	0.0313	0.0320	0.0329	0.0324
Cu–Cl	0.0596	0.0418	0.0397	0.0114	0.0490	0.0381	0.0419	0.0391	0.0394

vacant $[Cu(L)]^+$ species without the fifth axial Cu^{I}–Cl bond,[26] which were confirmed by the methyl and phenyl substituted TPA copper(I) complexes, $[Cu(TPA^{Me})]^+[ClO_4^-]$,[27] $[Cu(TPA^{Ph})]^+[BPh_4^-]$[28] [$TPA^{Me}$ = tris(6-methyl-2-pyridylmethyl)amine, TPA^{Ph} = tris(6- phenyl-2-pyridylmethyl)amine], and tris(2-dimethylaminoethyl)amine (TEA^{Me2}) copper(I) complex $[Cu(TEA^{Me2})]^+[ClO_4^-]$.[29] However, a significantly elongated Cu–$N_{(axial)}$ bond distance (2.437 Å) is presented in the parent Cu^{I}(TPA)Cl compared to other three equatorial Cu–N_{py} bond distances (~ 2.08 Å), which suggests the parent Cu^{I}(TPA)Cl is best described as $[Cu^{I}(TPA\text{-}k^3N)Cl]$, a tetra-coordinated Cu^{I}–Cl complex.[30] The Cu^{I}–Cl bond in Cu^{I}(TPA)Cl was stabilized by C–H···Cl interaction,[31] which was proven by the related bond critical points from AIM (atoms in molecules) analysis (see Figure 2, and below discussion). Even more elongated Cu–Cl bond in $Cu^{I}(TPA^{OH})Cl$ (2.566 Å) compared to that in the parent Cu^{I}(TPA)Cl (2.398 Å) was observed in the solid-state X-ray structure. However, a shortened Cu–$N_{(axial)}$ bond in $Cu^{I}(TPA^{OH})Cl$ (2.238 Å)[6] compared to that in the parent Cu^{I}(TPA)Cl (2.437 Å)[7] was observed. The Cu–$N_{(axial)}$ and Cu–Cl bond distances in the $Cu^{I}(TPA^{NHPh})Cl$ are 2.252 and 2.339 Å, respectively.[5] The values of τ_5 for $Cu^{I}(TPA^{OH})Cl$ and $Cu^{I}(TPA^{NHPh})Cl$ are 0.95 and 1.12,[5–6] respectively, which demonstrate the existences of trigonal bipyramidal copper centers in these hydrogen-bond assisted Cu^{I}–Cl complexes.

The hydrogen-bond induced cage effects[32] on the chloride dissociation in the Cu^{I}(L)–Cl complexes are computationally evaluated. The Gibbs energies for chloride dissociation in the Cu^{I}(L)–Cl complexes from (SMD)-PBEPBE-D3BJ/Def2-TZVP//PBEPBE-D3BJ/Def-TZVP computations (ΔG^{1}_{RXN}, Scheme 2) present the following three findings: (1) for complexes **1**, **2**, and **3**, the $Cu^{I}(TPA^{OH})Cl$ complex **2** has the maximum Gibbs energy for chloride dissociation (26.4 kcal mol^{-1}), the parent Cu^{I}(TPA)Cl complex **1** shows the minimum Gibbs energy for chloride dissociation (12.2 kcal mol^{-1}), and the $Cu^{I}(TPA^{NH2})Cl$ complex **3** [TPA^{NH2} = tris(6-amino-2-pyridylmethyl)amine] has a slightly higher Gibbs energy (13.8 kcal mol^{-1}) than that of Cu^{I}(TPA)Cl complex **1** (12.2 kcal mol^{-1}). This trend is consistent with the relative bond strengths of O–H···Cl, N–H···Cl, and C–H···Cl bonds. AIM analyses[18] on the O–H···Cl, N–H···Cl, and C–H···Cl bonds in the Cu^{I}(L)–Cl complexes are performed to investigate their bond strengths. The electron densities of O–H···Cl hydrogen bond (**2**), N–H···Cl hydrogen bond (**3**), and C–H···Cl weak hydrogen bond (**1**) critical points [$\rho_{(BCP)}$ (in a.u.)] are 0.0397, 0.0267 and 0.0108 (Table 1), respectively, which validate the maximum stabilization of O–H···Cl bonds in $Cu^{I}(TPA^{OH})Cl$ complex **2** for chloride dissociation. (2) for complexes **4**, **5**, **8**, and **9**, the more stabilized Cu^{I}–Cl bonds in complexes with introduced electron-withdrawing group (CF_3) compared to the electron-donating group (CH_3) are obtained. The Gibbs energies for chloride dissociation in complexes **5** $[Cu^{I}(TPA^{NHCF3})Cl]$, **8** $[Cu^{I}(TPA^{NHPhCF3})Cl]$, **4** $[Cu^{I}(TPA^{NHMe})Cl]$, and **9** $[Cu^{I}(TPA^{NHPh})Cl]$ are 22.7, 18.8, 15.6 and 13.6 kcal mol^{-1}, respectively. The electron densities of N–H···Cl hydrogen bond critical points $\rho_{(BCP)}$ in complexes **5**, **8**, **4**, and **9** are 0.0354, 0.0329, 0.0320 and 0.0324 (Table 1), respectively. Since the introduced electron-withdrawing groups in the Cu^{I}(L)–Cl complexes weaken the N–H bond, the stronger N–H···Cl hydrogen bonds with introduced electron-withdrawing CF_3 groups are anticipated and observed. (3) for complexes **4**, **5**, **6**, and **7**, the enhanced N–H···Cl hydrogen bond is benefited via directly introduced proximal electron-withdrawing groups compared to the introduced distal electron-withdrawing groups. The Cu^{I}–Cl bond in complex **5** with introduced proximal CF_3 groups $[Cu^{I}(TPA^{NHCF3})Cl$, 22.7 kcal mol$^{-1}]$ is 4.6 kcal mol^{-1} more stable than that of complex **7** $[Cu^{I}(TPA^{NH2CF3})Cl$, 18.1 kcal mol$^{-1}]$ with introduced distal CF_3 groups. Compared to complex **3** $[Cu^{I}(TPA^{NH2})Cl$, 13.8 kcal mol$^{-1}]$, no obvious effect for complex **6** $[Cu^{I}(TPA^{NH2Me})Cl$, 13.9 kcal mol^{-1}, TPA^{NH2Me} = tris(6-amino-4-methyl-2-pyridylmethyl)amine] with introduced distal electron-donating group in the stabilization of Cu^{I}–Cl bond is obtained. The electron densities of N–H···Cl hydrogen bond critical points $\rho_{(BCP)}$ in complexes **6** and **7** are 0.0313 and 0.0320, respectively (Table 1).

The relationship between the electron densities of N–H···Cl, O–H···Cl hydrogen bond critical points $\rho_{(BCP)}$ and the Gibbs energies of chloride dissociation (ΔG^{1}_{RXN}) is linearly fitted (Figure 1). A reasonable linear fitting between the $\rho_{(BCP)}$ and ΔG^{1}_{RXN} for the complexes **2** to **9** is obtained with R^2 value of 0.8584, and an excellent linear fitting between the $\rho_{(BCP)}$ and ΔG^{1}_{RXN} for the complexes **2** to **7** is presented with R^2 value of

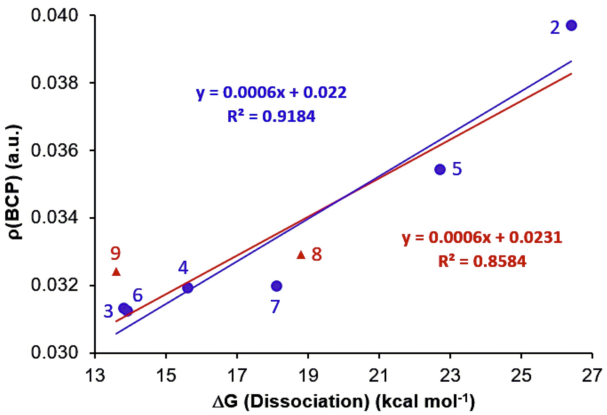

Figure 1. The linear fitting between $\rho_{(BCP)}$ and the Gibbs energy of Cl^- dissociation of Cu^{I}(L)–Cl. The blue line and blue equation represent the values for complexes **2** to **7**, and the red line and red equation represent the values for complexes **2** to **9**, and values from complex **1** are excluded due to its non-hydrogen bond.

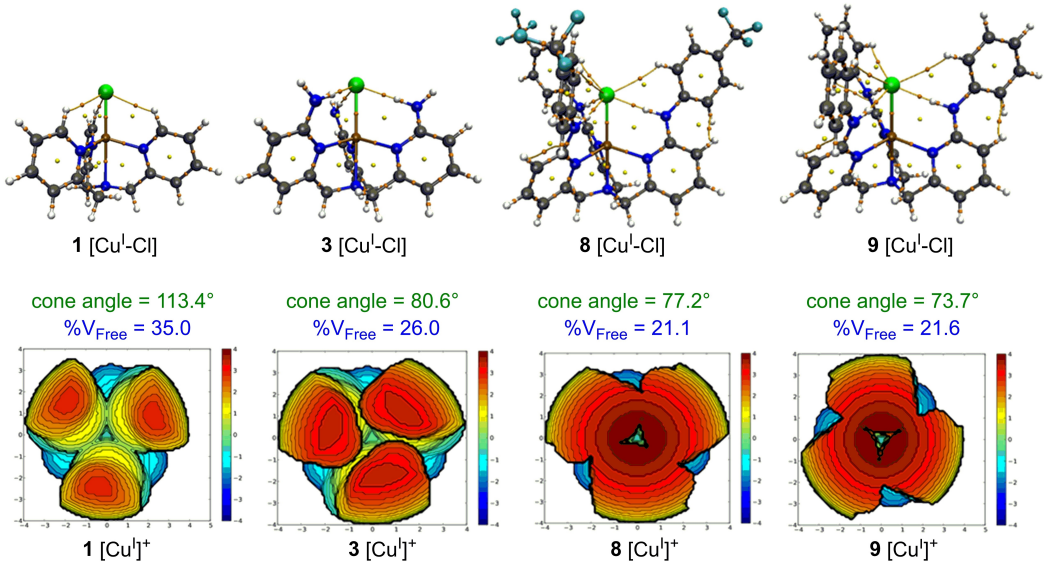

Figure 2. The critical points from AIM (Atoms-In-Molecules) analyses (top) and steric map (bottom) of **1**, **3**, **8** and **9**. Color codes for 3D structures: brown, Cu; blue N; black, C; white, H; red, O; green, Cl; cyan, F. The orange balls represent the BCP (bond critical point), the yellow balls represent ring critical point (RCP), and the bond paths for hydrogen bonds are shown in orange.

0.9184. Further AIM analyses on the bond critical points of complexes **8** and **9** show that the out-sphere distal C–H···Cl weak hydrogen bonds also participate in the stabilization of Cu^{I}–Cl bonds (Figure 2), besides the above-mentioned proximal N–H···Cl hydrogen bonding interactions. The electron densities of the distal C–H···Cl weak hydrogen bond critical points $\rho_{(BCP)}$ of complexes **8** and **9** are 0.0067 and 0.0063, respectively, which are even weaker than the C–H···Cl bond in the parent complex **1** [Cu^{I}(TPA)Cl, $\rho_{(BCP)}$ = 0.0108]. The exponential curve fitting between the electron densities of N–H···Cl, O–H···Cl hydrogen bond critical points $\rho_{(BCP)}$ and the Gibbs energies of chloride dissociation (ΔG^{1}_{RXN}) is also fitted (Figure S5). It is noted that improved exponential fittings for complexes **2** to **9** with R^2 value of 0.8683 and for complexes **2** to **7** with R^2 value of 0.9297 are presented. No reasonable fitting between the electron density of Cu–Cl bond critical points $\rho_{(BCP)}$ and ΔG^{1}_{RXN} could be established, neither the fitting between Cu–Cl bond distances and ΔG^{1}_{RXN}, nor the fitting between APT (atomic polar tensor) charge of Cu atom in the Cu^{I}(L)–Cl complexes **2** to **9** (R^2 < 0.2, Figures S6–S8).

Moreover, the multiple parameters equations are explored in the chloride dissociation (Scheme 3). An improved fitting of chloride dissociation (ΔG^{1}_{RXN}) including electron densities of hydrogen bond critical points $\rho_{(BCP)}$ and the APT charge of Cu atom in the Cu^{I}(L)–Cl complexes **2** to **9** is discovered (R^2 = 0.8611, Eq. 1, Scheme 3). The positive correlation between the $\rho_{(BCP)}$ and ΔG^{1}_{RXN} in Eq. 1 is presented via the positive coefficient (1506.5257), which indicates that Cu^{I}–Cl bonds could be stabilized by the hydrogen bonding interactions. The negative coefficient (−6.4198) between the APT charge of Cu atom and ΔG^{1}_{RXN} in Eq. 1 shows the negative correlation of APT charge of Cu atom on the ΔG^{1}_{RXN}. A more electron-rich Cu atom in the Cu^{I}(L)–Cl complex could form a weaker Cu^{I}–Cl bond and make

$$\Delta G^{1}_{RXN} = \mathrm{APT}(-6.4198) + \rho_{(BCP)}(1506.5257) - 30.1145 \quad \text{Eq. 1}$$
$$R^2 = 0.8611$$

$$\Delta G^{1}_{RXN} = \mathrm{APT}(-26.1826) + \rho_{(BCP)}(1440.2485) + \mathrm{Dis}(-3.4756) - 11.6043 \quad \text{Eq. 2}$$
$$R^2 = 0.8773$$

$$\Delta G^{2}_{RXN} = \mathrm{APT}(-158.5495) + \mathrm{Vol}(0.7968) + 1.9582 \quad \text{Eq. 3}$$
$$R^2 = 0.7051$$

$$\Delta G^{2}_{RXN} = \mathrm{APT}(-151.2617) + \mathrm{Vol}(1.1606) + \mathrm{Dis}(47.1291) - 111.5009 \quad \text{Eq. 4}$$
$$R^2 = 0.7194$$

Scheme 3. The multiple parameters models of the Gibbs reaction energies. In Eq. 1 and 2, APT is APT charge of Cu atom in the [Cu^{I}–Cl], Dis is the Cu–Cl bond distance in the [Cu^{I}–Cl], and $\rho_{(BCP)}$ is the electron densities of hydrogen bond critical points. In Eq. 3 and 4, APT is APT charge of Cu atom in the [Cu^{I}]$^{+}$, Dis is the Cu–$N_{(axial)}$ bond distance in the [Cu^{I}]$^{+}$, and Vol is the percentages of free volume (%V_{Free}) of [Cu^{I}]$^{+}$.

the chloride dissociation easier. Another slightly improved three-parameter fitting of ΔG^{1}_{RXN} including electron densities of hydrogen bond critical points $\rho_{(BCP)}$, the APT charge of Cu atom and Cu–Cl bond distance in the Cu^{I}(L)–Cl complexes **2** to **9** is also observed (R^2 = 0.8773, Eq. 2, Scheme 3). It worth noting that the trend of chloride dissociation (ΔG^{1}_{RXN}) in the hydrogen bonds stabilized complexes **2** to **9** is improved by multiple-parameter structure-activity models (Scheme 3) compared to the one-parameter fitting (Figures 1 and S5), and a more accurate multiple-parameter structure-activity model could be achieved by expanding the number of models in this test set.

Formation of trans-1,2-peroxodicopper $[Cu_2–O_2]^{2+}$ (ΔG^{2}_{RXN})

The above discussions show that the Cu^{I}–Cl bonds are stabilized by intramolecular O–H···Cl and N–H···Cl hydrogen bonds, Cl atom is captured by the cage formed by out-sphere

Table 2. The calculated steric parameters of $Cu^{I}(L)^{+}$.

Parameter	1	2	3	4	5	6	7	8	9
Cone angle	113.4	79.9	80.6	80.4	73.6	75.3	80.5	77.2	73.7
$\%V_{Free}$	35.0	27.3	26.0	25.8	24.1	26.0	26.1	21.1	21.6
$\%V_{Buried}$	65.0	72.7	74.0	74.2	75.9	74.0	73.9	78.9	78.4

hydrogen bonds, and no spontaneously favorable chloride dissociation could be achieved in the $Cu^{I}(L)$–Cl complexes (ΔG^{1}_{RXN}, Scheme 2). In order to form the *trans*-1,2-peroxodicopper complex $[\{Cu(TPA^{NHPh})\}_2(\mu\text{-}1,2\text{-}O_2)]^{2+}[BAr^{-}]_2$ [BAr=$B(C_6F_5)_4^{-}$] (Scheme 1), the axially vacant $[Cu(TPA^{NHPh})]^{+}[BAr]$ was prepared separately and then reacted with dry O_2 in CH_2Cl_2 solution at −70 °C.[5] The formation of other *trans*-1,2-peroxodicopper complexes could be achieved through the similar O_2 binding to the axially vacant $[Cu(L)]^{+}[BAr^{-}]$. The formation of *trans*-1,2-peroxodicopper complexes via O_2 binding to the axially vacant $[Cu(L)]^{+}[BAr^{-}]$ is demonstrated as a favorable spontaneous reaction by the computed Gibbs reaction energies (ΔG^{2}_{RXN}, Scheme 2). The electronic effect and steric hindrance in the formation of *trans*-1,2-peroxodicopper complexes are investigated. To quantitatively evaluate the steric hindrances, the estimated cone angles,[33] the percentage buried volume ($\%V_{Bur}$),[24] the O_2 accessible free volume ($\%V_{Free}$), and steric map[25] were calculated and presented (Figure 2, Table 2 and S7–S9).

The maximum estimated cone angle (113.4°) is observed in the parent unsubstituted axially vacant **1** $[Cu^{I}]^{+}$ $[Cu(TPA)]^{+}$, and relatively small cone angles present in **2** $[Cu^{I}]^{+}$ $[Cu(TPA^{OH})]^{+}$ and **5** $[Cu^{I}]^{+}$ $[Cu(TPA^{NHCF3})]^{+}$ containing the strong O–H···Cl and N–H···Cl hydrogen bonding in the related $Cu^{I}(L)$–Cl complexes (79.9° for **2** $[Cu^{I}]^{+}$ and 73.6° for **5** $[Cu^{I}]^{+}$) (Table 2). The similar trend in the calculated O_2 accessible free volume ($\%V_{Free}$, 35.0 for **1** $[Cu^{I}]^{+}$, 27.3 for **2** $[Cu^{I}]^{+}$ and 24.1 for **5** $[Cu^{I}]^{+}$) is also observed (Table 2). It is surprising that no reasonable fitting between the Gibbs energies for the formation of *trans*-1,2-peroxodicopper complexes (ΔG^{2}_{RXN}) and the steric hindrances (cone angles or accessible free volume $\%V_{Free}$) could be established, neither the fitting between ΔG^{2}_{RXN} and APT charge of Cu atom in the $[Cu^{I}]^{+}$ complexes (Figures S14–S16). This finding suggests that multiple factors exist in the formation of *trans*-1,2-peroxodicopper complex $[Cu_2–O_2]^{2+}$ via the O_2 binding to the axially vacant $[Cu(L)]^{+}[BAr^{-}]$. To evaluate the steric hindrance and electronic effect in the formation of *trans*-1,2-peroxodicopper $[Cu_2–O_2]^{2+}$, the two-parameter model between the ΔG^{2}_{RXN} and the O_2 accessible free volume $\%V_{Free}$ and APT charge of Cu atom in the $Cu^{I}(L)^{+}$ is fitted ($R^2=0.7051$, Eq. 3, Scheme 3). This reasonable fitting demonstrates the positive correlation of O_2 accessible free volume $\%V_{Free}$ and the negative correlation of APT charge of Cu atom on the ΔG^{2}_{RXN}. It shows that the electron-rich Cu atom is unfavorable to form the Cu–O bond in the *trans*-1,2-peroxodicopper complex $[Cu_2–O_2]^{2+}$ via the electrostatic repulsion. The O_2 binding to the axially vacant $[Cu(L)]^{+}[BAr^{-}]$ is benefited by the high O_2 accessible free volume $\%V_{Free}$ of the axially vacant $[Cu(L)]^{+}[BAr^{-}]$. Another slightly improved three-parameter model of ΔG^{2}_{RXN} including O_2 accessible free volume $\%V_{Free}$, APT charge of Cu atom in the $Cu^{I}(L)^{+}$ and $Cu–N_{(axial)}$ bond distance in the $Cu^{I}(L)^{+}$ complexes **2** to **9** is also fitted ($R^2=0.7194$, Eq. 4, Scheme 3).

The most favorable formation of *trans*-1,2-peroxodicopper complexes among the amine substituted TPA complexes **3** $[Cu^{I}]^{+}$ to **9** $[Cu^{I}]^{+}$ is **8** $[Cu^{I}]^{+}$ $[Cu^{I}(TPA^{NHPhCF3})]^{+}$ (−15.1 kcal mol^{-1}), which has a lower ΔG^{2}_{RXN} compared to that of 9 $[Cu^{I}]^{+}$ $[Cu^{I}(TPA^{NHPh})]^{+}$ (−11.6 kcal mol^{-1}, Scheme 2). Comparison between ΔG^{2}_{RXN} of **1** $[Cu^{I}]^{+}$ (−7.1 kcal mol^{-1}) and **3** $[Cu^{I}]^{+}$ (−5.0 kcal mol^{-1}, Scheme 2) suggests the importance of electronic nature of ligand in the formation of *trans*-1,2-peroxodicopper complexes. As an electron-donating groups, amine substituted TPA ligand (**3**, TPA^{NH2}) generates an electron-rich Cu atom, which prevents the O_2 binding to the axially vacant $[Cu(L)]^{+}[BAr^{-}]$. It is verified by the longer Cu–O bond in the *trans*-1,2-peroxodicopper complexes **3** $[Cu_2–O_2]^{2+}$ (1.943 Å, Scheme S2) and **1** $[Cu_2–O_2]^{2+}$ (1.936 Å, Scheme S2). The comparison between the formation of **3** $[Cu_2–O_2]^{2+}$ and **1** $[Cu_2–O_2]^{2+}$ suggests the competition between hydrogen bond interaction and the electronic effect. A long Cu–O bond in the *trans*-1,2-peroxodicopper complex involved strong N–H···O hydrogen bonds **2** $[Cu_2–O_2]^{2+}$ is observed (2.005 Å, Scheme S2), and the formation of **2** $[Cu_2–O_2]^{2+}$ (−16.0 kcal mol^{-1}, Scheme 2) is more favorable compared to that of **3** $[Cu_2–O_2]^{2+}$ (−5.0 kcal mol^{-1}) and **1** $[Cu_2–O_2]^{2+}$ (−7.1 kcal mol^{-1}, Scheme 2). The O_2 accessible free volumes ($\%V_{Free}$) of **1** $[Cu^{I}]^{+}$, **2** $[Cu^{I}]^{+}$ and **3** $[Cu^{I}]^{+}$ are 35.0, 27.3 and 26.0, respectively (Table 2). The C–H···O weak hydrogen bonds in **1** $[Cu_2–O_2]^{2+}$ ($\rho_{(BCP)}=0.0101$), the O–H···O strong hydrogen bonds in **2** $[Cu_2–O_2]^{2+}$($\rho_{(BCP)}=0.0447$) and N–H···O strong hydrogen bonds in **3** $[Cu_2–O_2]^{2+}$ ($\rho_{(BCP)}=0.0316$) are illustrated in Figure 3. The above analyses on the **1** $[Cu_2–O_2]^{2+}$, **2** $[Cu_2–O_2]^{2}$ and **3** $[Cu_2–O_2]^{2+}$ demonstrate the critical role of intramolecular hydrogen bonds in the formation of *trans*-1,2-peroxodicopper complexes.

The steric hindrances of **8** $[Cu^{I}]^{+}$ and **9** $[Cu^{I}]^{+}$ are significantly stronger that other $[Cu^{I}]^{+}$ complexes, which are proven by the O_2 accessible free volumes ($\%V_{Free}$) of **8** $[Cu^{I}]^{+}$ (21.4, Figure 2) and **9** $[Cu^{I}]^{+}$ (21.6, Figure 2). AIM (Atoms-In-

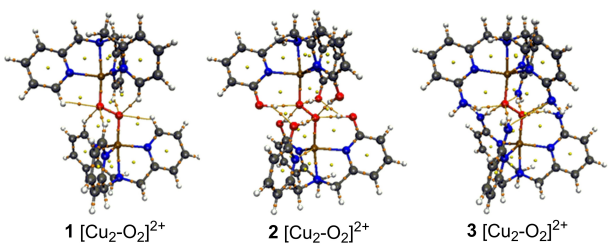

Figure 3. The critical points of *trans*-1,2-peroxodicopper complexes **1**, **2** and **3**.

Molecules) analyses on the critical points of **8** $[Cu_2–O_2]^{2+}$ and **9** $[Cu_2–O_2]^{2+}$ show that the additional distal intramolecular C–H···N weak hydrogen bonds are also involved in the stabilization of the *trans*-1,2-peroxodicopper complexes, besides the major contribution from the proximal N–H···O hydrogen bonds (Table S10). The averaged $\rho_{(BCP)}$ of the distal C–H···N weak hydrogen bonds in **8** $[Cu_2–O_2]^{2+}$ and **9** $[Cu_2–O_2]^{2+}$ are 0.0092, and 0.0083, respectively, which are weaker than the C–H···O weak hydrogen bond in **1** $[Cu_2–O_2]^{2+}$($\rho_{(BCP)}$ = 0.0101, Figure 3). The averaged $\rho_{(BCP)}$ of the major proximal N–H···O hydrogen bonds in **8** $[Cu_2–O_2]^{2+}$ and **9** $[Cu_2–O_2]^{2+}$ are 0.0332, and 0.0349 (Table S10), respectively, which are stronger than the N–H···O hydrogen bond in **3** $[Cu_2–O_2]^{2+}$ ($\rho_{(BCP)}$ = 0.0316, Figure 3). The computational results on **8** $[Cu_2–O_2]^{2+}$ and **9** $[Cu_2–O_2]^{2+}$ confirmed the hypothesis of critical participation of intramolecular hydrogen bonds in the stabilization of *trans*-1,2-peroxodicopper complexes.[5–6]

Conclusion

The critical roles of intramolecular hydrogen bonds in the stabilization of Cu^{I}–Cl bonds in the Cu^{I}(L)–Cl complexes and in the formation of stable *trans*-1,2-peroxodicopper complexes are computationally investigated in this contribution. The strength of hydrogen bond is evaluated by the electron density of bond critical points $\rho_{(BCP)}$ from AIM analysis. The reasonable two-parameter structure-activity model (R^2 = 0.8611) and three-parameter structure-activity model (R^2 = 0.8773) for chloride dissociation (ΔG^1_{RXN}) in the hydrogen bonds stabilized complexes **2** to **9** were established, which include the electron densities of hydrogen bond critical points $\rho_{(BCP)}$, APT charge of Cu atom and Cu–Cl bond distance. The O_2 accessible free volume ($\%V_{Free}$) and steric map are calculated to evaluate the steric hindrances of various tetradentate N-donor ligands. Acceptable two-parameter structure-activity model (R^2 = 0.7051) for the formation of *trans*-1,2-peroxodicopper complexes via O_2 binding (ΔG^1_{RXN}) is also obtained. Despite the strong steric hindrances of **8** $[Cu^{I}]^+$ ($\%V_{Free}$ = 21.4) and **9** $[Cu^{I}]^+$ ($\%V_{Free}$ = 21.6), the favorable formation of stable *trans*-1,2-peroxodicopper complexes **8** $[Cu_2–O_2]^{2+}$ (-15.1 kcal mol^{-1}) and **9** $[Cu_2–O_2]^{2+}$ (-11.6 kcal mol^{-1}) are obtained. The reasonable structure-activity models from DFT computations provide the fundamental insights into the structures of *trans*-1,2-peroxodicopper mimics, and promote the design of hydrogen-bondassisted *trans*-1,2-peroxodicopper intermediate in the copper catalyzed O_2 oxygenation.

Acknowledgements

We thank the Mississippi Center for Supercomputing Research (MCSR) for computing support. We thank the Department of Chemistry at Mississippi State University, and the Department of Chemistry at the University of Michigan.

Conflict of Interest

The authors declare no conflict of interest.

Keywords: Atoms-in-molecules theory · *Trans*-1,2-peroxodicopper · Density functional calculations · Hydrogen bonds · Structure-activity model

[1] a) E. I. Solomon, D. E. Heppner, E. M. Johnston, J. W. Ginsbach, J. Cirera, M. Qayyum, M. T. Kieber-Emmons, C. H. Kjaergaard, R. G. Hadt, L. Tian, *Chem. Rev.* **2014**, *114*, 3659–3853; b) R. Trammell, K. Rajabimoghadam, I. Garcia-Bosch, *Chem. Rev.* **2019**, *119*, 2954–3031; c) Y. Liang, J. Wei, X. Qiu, N. Jiao, *Chem. Rev.* **2018**, *118*, 4912–4945; d) P. Chen, E. I. Solomon, *Proc. Natl. Acad. Sci. USA* **2004**, *101*, 13105–13110; e) R. E. Cowley, L. Tian, E. I. Solomon, *Proc. Natl. Acad. Sci. USA* **2016**, *113*, 12035–12040.

[2] a) E. I. Solomon, U. M. Sundaram, T. E. Machonkin, *Chem. Rev.* **1996**, *96*, 2563–2606; b) L. M. Mirica, X. Ottenwaelder, T. D. P. Stack, *Chem. Rev.* **2004**, *104*, 1013–1046; c) S. M. Adam, G. B. Wijeratne, P. J. Rogler, D. E. Diaz, D. A. Quist, J. J. Liu, K. D. Karlin, *Chem. Rev.* **2018**, *118*, 10840–11022.

[3] a) C. E. Elwell, N. L. Gagnon, B. D. Neisen, D. Dhar, A. D. Spaeth, G. M. Yee, W. B. Tolman, *Chem. Rev.* **2017**, *117*, 2059–2107; b) D. Maiti, J. S. Woertink, A. A. Narducci Sarjeant, E. I. Solomon, K. D. Karlin, *Inorg. Chem.* **2008**, *47*, 3787–3800; c) Y. Lee, G. Y. Park, H. R. Lucas, P. L. Vajda, K. Kamaraj, M. A. Vance, A. E. Milligan, J. S. Woertink, M. A. Siegler, A. A. Narducci Sarjeant, L. N. Zakharov, A. L. Rheingold, E. I. Solomon, K. D. Karlin, *Inorg. Chem.* **2009**, *48*, 11297–11309; d) M. T. Kieber-Emmons, J. W. Ginsbach, P. K. Wick, H. R. Lucas, M. E. Helton, B. Lucchese, M. Suzuki, A. D. Zuberbühler, K. D. Karlin, E. I. Solomon, *Angew. Chem. Int. Ed.* **2014**, *53*, 4935–4939; *Angew. Chem.* **2014**, *126*, 5035–5039; e) S. Itoh, Y. Tachi, *Dalton Trans.* **2006**, 4531–4538; f) A. Hoffmann, M. Wern, T. Hoppe, M. Witte, R. Haase, P. Liebhäuser, J. Glatthaar, S. Herres-Pawlis, S. Schindler, *Eur. J. Inorg. Chem.* **2016**, *2016*, 4744–4751; g) M. Lerch, M. Weitzer, T.-D. J. Stumpf, L. Laurini, A. Hoffmann, J. Becker, A. Miska, R. Göttlich, S. Herres-Pawlis, S. Schindler, *Eur. J. Inorg. Chem.* **2020**, *2020*, 3143–3150.

[4] a) S. Yamaguchi, S. Nagatomo, T. Kitagawa, Y. Funahashi, T. Ozawa, K. Jitsukawa, H. Masuda, *Inorg. Chem.* **2003**, *42*, 6968–6970; b) A. Chapovetsky, M. Welborn, J. M. Luna, R. Haiges, T. F. Miller, S. C. Marinescu, *ACS Cent. Sci.* **2018**, *4*, 397–404; c) E. W. Dahl, J. J. Kiernicki, M. Zeller, N. K. Szymczak, *J. Am. Chem. Soc.* **2018**, *140*, 10075–10079; d) S. Kim, C. Saracini, M. A. Siegler, N. Drichko, K. D. Karlin, *Inorg. Chem.* **2012**, *51*, 12603–12605; e) Y. J. Park, N. S. Sickerman, J. W. Ziller, A. S. Borovik, *Chem. Commun.* **2010**, *46*, 2584–2586; f) N. S. Sickerman, Y. J. Park, G. K. Y. Ng, J. E. Bates, M. Hilkert, J. W. Ziller, F. Furche, A. S. Borovik, *Dalton Trans.* **2012**, *41*, 4358–4364.

[5] E. W. Dahl, H. T. Dong, N. K. Szymczak, *Chem. Commun.* **2018**, *54*, 892–895.

[6] C. M. Moore, D. A. Quist, J. W. Kampf, N. K. Szymczak, *Inorg. Chem.* **2014**, *53*, 3278–3280.

[7] W. T. Eckenhoff, T. Pintauer, *Inorg. Chem.* **2007**, *46*, 5844–5846.

[8] A. Wada, Y. Honda, S. Yamaguchi, S. Nagatomo, T. Kitagawa, K. Jitsukawa, H. Masuda, *Inorg. Chem.* **2004**, *43*, 5725–5735.

[9] M. J. Frisch, G. W. Trucks, H. B. Schlegel, G. E. Scuseria, M. A. Robb, J. R. Cheeseman, G. Scalmani, V. Barone, G. A. Petersson, H. Nakatsuji, X. Li, M. Caricato, A. V. Marenich, J. Bloino, B. G. Janesko, R. Gomperts, B. Mennucci, H. P. Hratchian, J. V. Ortiz, A. F. Izmaylov, J. L. Sonnenberg, D. Williams-Young, F. Ding, F. Lipparini, F. Egidi, J. Goings, B. Peng, A. Petrone, T. Henderson, D. Ranasinghe, V. G. Zakrzewski, J. Gao, N. Rega, G. Zheng, W. Liang, M. Hada, M. Ehara, K. Toyota, R. Fukuda, J. Hasegawa, M. Ishida, T. Nakajima, Y. Honda, O. Kitao, H. Nakai, T. Vreven, K. Throssell, J. A. Montgomery Jr., J. E. Peralta, F. Ogliaro, M. J. Bearpark, J. J. Heyd, E. N. Brothers, K. N. Kudin, V. N. Staroverov, T. A. Keith, R. Kobayashi, J. Normand, K. Raghavachari, A. P. Rendell, J. C. Burant, S. S. Iyengar, J. Tomasi, M. Cossi, J. M. Millam, M. Klene, C. Adamo, R. Cammi, J. W. Ochterski, R. L. Martin, K. Morokuma, O. Farkas, J. B. Foresman, D. J. Fox, *Gaussian 16, Revision C.01*, Gaussian, Inc., Wallingford, CT, **2019**.

[10] a) J. P. Perdew, K. Burke, M. Ernzerhof, *Phys. Rev. Lett.* **1996**, *77*, 3865–3868; b) J. P. Perdew, K. Burke, M. Ernzerhof, *Phys. Rev. Lett.* **1997**, *78*, 1396.

[11] A. Schäfer, C. Huber, R. Ahlrichs, *J. Chem. Phys.* **1994**, *100*, 5829–5835.

[12] S. Grimme, J. Antony, S. Ehrlich, H. Krieg, *J. Chem. Phys.* **2010**, *132*, 154104.
[13] S. Grimme, S. Ehrlich, L. Goerigk, *J. Comput. Chem.* **2011**, *32*, 1456–1465.
[14] a) B. I. Dunlap, *J. Chem. Phys.* **1983**, *78*, 3140–3142; b) B. I. Dunlap, *J. Mol. Struct.* **2000**, *529*, 37–40.
[15] D. G. Liakos, F. Neese, *J. Chem. Theory Comput.* **2011**, *7*, 1511–1523.
[16] F. Weigend, R. Ahlrichs, *Phys. Chem. Chem. Phys.* **2005**, *7*, 3297–3305.
[17] A. V. Marenich, C. J. Cramer, D. G. Truhlar, *J. Phys. Chem. B* **2009**, *113*, 6378–6396.
[18] a) R. F. W. Bader, *Acc. Chem. Res.* **1985**, *18*, 9–15; b) R. F. W. Bader, *Atoms in Molecules: A Quantum Theory*, Oxford University Press, Oxford, **1990**; c) R. F. W. Bader, *Chem. Rev.* **1991**, *91*, 893–928.
[19] F. Fuster, B. Silvi, *Theor. Chem. Acc.* **2000**, *104*, 13–21.
[20] T. Lu, F. Chen, *J. Comput. Chem.* **2012**, *33*, 580–592.
[21] W. Humphrey, A. Dalke, K. Schulten, *J. Mol. Graphics* **1996**, *14*, 33–38.
[22] C. F. Macrae, I. Sovago, S. J. Cottrell, P. T. A. Galek, P. McCabe, E. Pidcock, M. Platings, G. P. Shields, J. S. Stevens, M. Towler, P. A. Wood, *J. Appl. Crystallogr.* **2020**, *53*, 226–235.
[23] a) L. Falivene, R. Credendino, A. Poater, A. Petta, L. Serra, R. Oliva, V. Scarano, L. Cavallo, *Organometallics* **2016**, *35*, 2286–2293; b) *SambVca, version 2.1. https://www.molnac.unisa.it/OMtools/sambvca2.1/index.html*, **2019**; c) L. Falivene, Z. Cao, A. Petta, L. Serra, A. Poater, R. Oliva, V. Scarano, L. Cavallo, *Nat. Chem.* **2019**, *11*, 872–879.
[24] A. Poater, F. Ragone, S. Giudice, C. Costabile, R. Dorta, S. P. Nolan, L. Cavallo, *Organometallics* **2008**, *27*, 2679–2681.
[25] A. Poater, F. Ragone, R. Mariz, R. Dorta, L. Cavallo, *Chem. Eur. J.* **2010**, *16*, 14348–14353.
[26] a) T. J. Zerk, P. V. Bernhardt, *Coord. Chem. Rev.* **2018**, *375*, 173–190; b) C. Bravin, E. Badetti, G. Licini, C. Zonta, *Coord. Chem. Rev.* **2021**, *427*, 213558.
[27] H. Hideki, U. Kounosuke, F. Shuhei, N. Shigenori, S. Kazushi, F. Hideki, S. Masatatsu, U. Akira, K. Teizo, *Chem. Lett.* **2002**, *31*, 416–417.
[28] C.-I. Chuang, K. Lim, Q. Chen, J. Zubieta, J. W. Canary, *Inorg. Chem.* **1995**, *34*, 2562–2568.
[29] M. Becker, F. W. Heinemann, S. Schindler, *Chem. Eur. J.* **1999**, *5*, 3124–3129.
[30] W. T. Eckenhoff, T. Pintauer, *Inorg. Chem.* **2010**, *49*, 10617–10626.
[31] a) C. B. Aakeröy, T. A. Evans, K. R. Seddon, I. Pálinkó, *New J. Chem.* **1999**, *23*, 145–152; b) M. Ikeda, A. K. Sah, M. Iwase, R. Murashige, J.-i. Ishi-i, M. Hasegawa, C. Kachi-Terajima, K.-M. Park, S. Kuwahara, Y. Habata, *Dalton Trans.* **2017**, *46*, 3800–3804.
[32] Y. Liu, W. Zhao, C.-H. Chen, A. H. Flood, *Science* **2019**, *365*, 159–161.
[33] a) C. A. Tolman, *Chem. Rev.* **1977**, *77*, 313–348; b) C. A. Tolman, W. C. Seidel, L. W. Gosser, *J. Am. Chem. Soc.* **1974**, *96*, 53–60; c) C. A. Tolman, *J. Am. Chem. Soc.* **1970**, *92*, 2956–2965.

Manuscript received: March 1, 2021
Revised manuscript received: April 24, 2021
Accepted manuscript online: April 28, 2021